Characterizing the tissue of apple air-dried and osmo-air-dried rings by X-ray CT and OCT and relationship with ring crispness and fruit maturity at harvest measured by TRS.

Anna Rizzolo[a], Maristella Vanoli[a,b], Giovanna Cortellino[a], Lorenzo Spinelli[c], Davide Contini[b], Els Herremans[d], Evi Bongaers[e], Alexandra Nemeth[f], Michael Leitner[f], Pieter Verboven[e], Bart M. Nicolaï[e], Alessandro Torricelli[b]

[a] Consiglio per la Ricerca e Sperimentazione in Agricoltura, Unità di ricerca per i processi dell'industria agroalimentare (CRA-IAA), via Venezian 26, 20133 Milano, Italy

[b] Politecnico di Milano, Dipartimento di Fisica, piazza Leonardo da Vinci 32, 20133 Milano, Italy

[c] Istituto di Fotonica e Nanotecnologie, CNR, piazza Leonardo da Vinci 32, 20133 Milano, Italy

[d] BIOSYST-MeBioS, KU Leuven, Willem de Croylaan 42 - box 2428, 3001 Leuven, Belgium

[e] Skyscan Bruker Micro-CT, Kartuizersweg 3B, 2550 Kontich, Belgium

[f] RECENDT, Research Center for Non Destructive Testing GmbH, Science Park 2/2, OG, Altenberger Straße 69, A-4040 Linz, Austria

corresponding author:

Anna Rizzolo, Consiglio per la Ricerca e Sperimentazione in Agricoltura, Unità di ricerca per i processi dell'industria agroalimentare (CRA-IAA), via Venezian 26, 20133 Milano, Italy; Phone: +39-02-239557213, e-mail: anna.rizzolo@entecra.it

Abstract

Air-dried apple rings were prepared from 'Golden Delicious' apples selected at harvest as less mature and more mature according to the absorption coefficient measured at 670 nm by TRS, stored in air for 5 months, and subjected to air-drying with (OSMO) and without (noOSMO) osmodehydration pre-treatment (60% sucrose syrup). Selected rings were submitted to microstructural analysis by X-ray computed tomography (X-ray CT), to subsurface structure analysis by Optical coherence tomography (OCT) and to texture and sound emission analysis by bending-snapping test. Higher crispness index, higher number of sound events and higher average SPL characterized the OSMO rings. Total porosity was related to $SPL_{av<60}$, tissue and pore anisotropy to $SPL_{av>60}$, pore fragmentation index to fracturability and specific surface area to the work required to snap the ring. A differentiation of the drying treatments, as well as of the products according to the TRS maturity class at harvest were obtained analysing by PCA microstructure parameters and texture and acoustic parameters. The differences in mechanical and acoustic characteristics between OSMO and noOSMO rings were due to the different subsurface structure as found with OCT analysis.

Key words: Microstructure, X-CT, OCT, raw material selection, TRS, acoustic-mechanical properties, crispness, osmodehydration pre-treatment, air-dried apple rings

Industrial relevance

There is an increasing demand of dried crispy fruit as they are considered by consumers healthy, natural and tasty foods. The textural characteristics, exerting a strong effect on crispy and crunchy sensory characteristics, have a great impact at consumption of dried crispy fruit. As their textural characteristics depend on both fruit maturity at processing and processing conditions, food industry is demanding nondestructive techniques which could be used for on-line/off-line sorting of fruit into classes each one more suited for obtaining a specific product. Furthermore, the textural properties of dried foods depend on microstructure, defined as the spatial arrangement of structural components and their interactions. Due to the microscopic complexity, unambiguous methodologies that relate quality to food microstructure do not

exist today, in contrast to what already existing for several engineering materials. Hence there is the need of developing methods that measure directly the microstructural properties of dried foods.

Highlights:

- For the first time, X-rayCT, OCT and acoustic emission coupled to texture analysis were combined to investigate the structure-property relationships of air-dried apple rings in relation to fruit maturity at harvest measured by TRS and to pre-drying osmodehydration.
- X-rayCT and OCT indicated changes in the microstructure related to crispness parameters measured by acoustic-texture analysis, which could be related to both fruit maturity at harvest and osmotic pre-treatment.
- The results show that a differentiation of the products according to the TRS maturity class at harvest was obtained.

1. **Introduction**

In the last few years, a new interest has arisen in the field of functional products, such as minimally processed fruits and vegetables. There is an increasing demand for innovative products that respond to changed lifestyles and working rhythms. In addition, consumers are also more and more interested in consuming healthy, natural and tasty foods. Dried crispy fruits could satisfy these requirements, as they are perceived as healthy because of their nutritional value, combined with high fiber content, but also tasty. Among these products, dried apples are part of several prepared foods including snack preparations and integral breakfast foods, as well they are used alone as snacks (Lewicki & Jakubczyk, 2004).

Drying is a process involving heat and mass transfer that can cause physical and chemical alteration of the material. The stress developed when water is removed from the fresh material causes shrinkage and change in shape, both of which influence the porosity of the dried material and its rehydration properties (Lewicki & Jakubczyk, 2004; Mayor, Silva & Sereno, 2005). Other consequences of the drying process involve changes in the rheological properties of the product, which are bound to changes in composition, phase transition of the material and microstructural changes due to loss of cell turgor pressure because of the loss of water from the inner parts towards the surface, possibly causing stiffness, spoilage and disruption of cell walls, or even a collapse of the cell tissue and a cell breakage (Lewicki & Lukaszuk, 2000; Maltini, Torreggiani, Venir & Bertolo, 2003). The extent of these changes depends on the species and on the maturation degree at processing, factors affecting the textural properties of the raw material.

The internal quality of fruit can be assessed non-destructively by using time-resolved reflectance spectroscopy (TRS), which provides a complete characterization of diffusive media with the simultaneous non-invasive measurement of the bulk optical properties. TRS is based on the measurement of the temporal delay and the broadening experienced by a short laser pulse (pulse duration in the order of 100 ps) while travelling through a turbid medium (Torricelli et al., 2008). By using an appropriate theoretical model of light penetration for the analysis of photon time distribution, it is possible to simultaneously estimate the absorption coefficient (μ_a) and the reduced scattering coefficient (μ'_s). Light penetration achieved by TRS in most fruit and vegetables can be as great as 1-2 cm, depending on the optical properties (Cubeddu et al., 2001). Hence, TRS provides information on the internal properties of the medium and is not significantly

affected by surface features (Saeys, Velazco-Roa, Thennadil, Ramon & Nicolaï, 2008). TRS has been used to assess maturity, texture and cell wall structure as well as internal defects in intact fruit (Vanoli, Zerbini, Rizzolo, Spinelli & Torricelli, 2010), and to sort fruit at harvest according to maturity class, usually by measuring fruit at 670 nm (near the chlorophyll-*a* peak) and classifying fruit with high μ_a670 values as less mature and those having low μ_a670 values as more mature (Torricelli et al., 2008). As for air-dried apple rings, it was shown that the classification of apples at harvest based on μ_a 670 was able to segregate fruit generating fresh and air-dried rings of different quality (Rizzolo, Vanoli, Cortellino, Spinelli & Torricelli, 2011; Rizzolo, Vanoli, Cortellino, Spinelli & Torricelli, 2012): the differences found in the raw material affected the changes occurring in apple rings with air-drying, mainly influencing weight loss, area shrinkage and how much ring color changed due to browning phenomena. For 'Golden Delicious' and 'Pink Lady®' cultivars, by processing the more mature fruits, i.e. either after long cold storage or by using apples having lower μ_a670 at harvest, air-dried rings with low shrinkage and low color changes (i.e. showing less browning) with lower ring hardness and crispness index were obtained.

However, maximal shrinkage during drying decreases as its solids increase and structure collapse was shown to decrease when fruit was impregnated with sugar prior to air drying (Torreggiani & Bertolo, 2004; Wolf, Behsnilian & Speiss, 2001) by means of an osmotic process, which is carried out by immerging the fruit into aqueous solutions of high sugar concentration, so achieving a partial dehydration coupled to a solute intake (Wolf, Behsnilian & Speiss, 2001). Moreover, great changes in the tissues structure could be produced by combining the osmotic dehydration with air drying (Lewicki, 1998), with texture changing from elastic-visco-plastic to rigid, becoming fragile and brittle, which are textural features linked to the crispy and crunchy sensory attributes proper of snack food (Saeleaw & Schleining, 2011). In addition, the rheological characteristics of osmo-air-dried apple rings were shown to change according to the cultivar: 'Golden Delicious' rings acquired rigidity but remained brittle and fragile, developing small fractures, whereas 'Pink Lady®' ones become rigid, but harder and stiffer, with abrupt failures of major intensity (Farris, Gobbi, Torreggiani & Piergiovanni, 2008; Gobbi, Farris, Limbo & Torreggiani, 2012). These mechanical characteristics are strictly bound to the porosity of dried apple rings, which has been characterized using different imaging 2-D techniques, such as light microscopy (Mayor, Silva & Sereno,

2005; Gobbi, Farris, Limbo & Torreggiani, 2012) and scanning electron microscopy (Bai, Rahaman, Perera, Smith & Melton, 2002; Acevedo, Briones, Buera & Aguilera, 2008; Askari, Eman-Djomeh & Mousavi, 2008; Witrowa-Rajchert & Rząca, 2009; Huang, Zhang, Wang, Mujumdar & Sun, 2012). Even if scanning electron microscopy is a useful tool to analyze the sample microstructure, it does not give reliable information about the total pore volume and pore size distribution in the sample. These information on the microstructure can be obtained using the X-ray microtomography, which has been applied to study the effect of far-infrared radiation assisted drying on microstructure of banana slices (Léonard, Blacher, Nimmol & Devahastin, 2007), and to quantify the pore space of apple tissue (Mendoza et al., 2007; Mendoza et al., 2010; Herremans et al., 2013).

Complementary information on dried ring microstructure could also be obtained using optical coherence tomography (OCT), a novel approach to assess the subsurface microstructure (Huang et al., 1991). OCT is a purely optical, non-destructive, non-invasive, and contactless high resolution imaging method, which is based on the physical phenomenon of white light interferometry. The technique employs special light sources with very short temporal coherence, which enables an excellent depth resolution in the range of only a few microns (Drexler et al., 1999). In the field of food and plant photonics so far OCT has been used to study the morphological and functional state of higher plant tissues (Sapozhnikova, Kamenskii & Kuranov, 2003; Kutis, Sapozhnikova, Kuranov & Kamenskii, 2005; Verboven et al., 2013) and to detect disease in melon seeds (Lee, Lee, Kim, Jung & Kim, 2011) and disease, defects and rots in onion (Meglinski, Buranachai & Terry, 2010; Landahl, Terry & Ford, 2012).

The objectives of this work were: a) to evaluate the subsurface structure and the microstructure of air-dried and osmo-air-dried apple rings by OCT and X-ray micro-tomography; and, b) to study the relationships among the microstructure features and the crispness of dried apple rings in relation to fruit maturity assessed at harvest by TRS.

2. **Materials and Methods**

2.1. *Fruit and experimental plan*

‘Golden Delicious’ apples (*Malus×domestica*, Borkh.) coming from Laimburg (Trentino Alto-Adige

region, Italy) were harvested on 8 September 2011, which corresponds to the commercial picking window for this cultivar in Trentino-Alto Adige region. Sixty fruits were selected and measured at harvest by TRS at 670 nm (close to the absorption peak of chlorophyll-*a*), ranked according to decreasing μ_a670 (increasing maturity) and randomized into three batches of 20 fruit each. The batches were stored for 5 months at +1°C in air. Each batch corresponded to a different pre-treatment: without osmodehydration pre-drying (noOSMO) and with 1 h (OSMO1) or 3 h (OSMO2) osmodehydration pre-drying. Three 5 mm thick rings/fruit were prepared. The rings from each fruit were packed together into a tulle bag and immersed for 1 h (OSMO1) or 3 h (OSMO2) at 20°C in a sucrose solution (a_w=0.90, 60% w/w), which was continuously recirculated at 1.5 L/min through a peristaltic pump. The ratio fruit/solution was 1/3. Before air drying, the OSMO rings were drained, rinsed gently with tap water, and placed a few minutes over adsorbent paper to remove excess water. OSMO and noOSMO rings were air-dried at 80°C up to a constant weight using a pilot alternate upward-downward air circulated drier (Thermolab, Codogno, Italy) operating at an air speed of 1.5 m/s.

Due to the duration of a single analysis, for the microstructural analysis by means of X-ray micro-CT a selection of dried apple samples was made: rings obtained from the most differing pre-treatments before drying (noOSMO and OSMO2) and from the most differing apples in terms of maturity measured by means of TRS (ranks 1 and 2, less mature (LeM) fruit and ranks 19 and 20, more mature (MoM) fruit) were chosen. For the subsurface microstructure analysis by OCT, instead, within each batch, the rings obtained from the most differing apples in terms of TRS maturity (rank 1, the least mature; rank 20, the most mature) were selected. On the dried rings prepared from the selected fruit, the mechanical and acoustic properties were measured using a texture analyzer in conjunction with acoustical emission analysis (bending-snapping test).

2.2. Assessment of maturity at harvest by time-resolved reflectance spectroscopy and samples formation

For TRS measurements, a compact system was used, working at 670 nm, based on a pulsed laser diode (mod. PDL800, PicoQuant GmbH, Germany), with 80 MHz repetition frequency, 100 ps duration, and 1

mW average power, a compact photomultiplier (mod. R5900U-L16, Hamamatsu Photonics, Japan) and an integrated PC board (mod. SPC130, Becker&Hickl GmbH, Germany). Typical acquisition time for time-correlated single photon counting is 1 s per point. A couple of 1 mm plastic fibers (Mod. ESKA GK4001, Mitsubishi, Japan) delivers light into the sample and collects the emitted photons at a distance of 1.5 cm. A band pass filter tuned at 670 nm was used to cut off the fluorescence signal due to chlorophyll. Overall, the instrumental response function duration was <160 ps. The reduced scattering coefficient (μ'_s) and the absorption coefficient (μ_a) were obtained by fitting the experimental TRS data with a standard solution of the diffusion approximation to the transport equation for a semi-infinite homogenous medium. The extrapolated boundary condition was used (Contini, Martelli, & Zaccanti, 1997) to take into account the refractive index mismatch at the surface.

The absorption coefficient at 670 nm was measured on two opposite sides of each fruit and the average per fruit was used for fruit ranking from less mature to more mature fruit. The 60 ranked apples were grouped by 3, with a total of 20 groups, corresponding to 20 levels of μ_a. Each fruit from each group was randomly assigned to a different pre-drying treatment. In this way, fruit from the whole range of μ_a were available for each pre-drying treatment.

2.3. Microstructural analysis

2.3.1 X-ray micro-CT

For the X-ray micro-CT analysis, by using a cork borer, small cylindrical samples (3 mm diameter) were excised from the dried apple, approximately 5 mm from the peel, excluding regions in which vascular tissue could be discerned visually. The thickness of the apple slices was not altered in preparing the samples. The samples were mounted on the rotating holder and stabilized using parafilm. Because of the dry state of the samples, hardly any sample degradation was expected within the time frame of the scan (29 minutes). X-ray micro-CT measurements were performed on a SkyScan 1172 system (Bruker microCT, Kontich, Belgium), operated at 55 keV source voltage and 181 µA current and with an isotropic image pixel resolution of 2.44 µm. The samples were rotated over 0.35° steps over a total of 180°, each time averaging 3 frames to acquire a radiographic image of 1048 by 2000 pixels. The projection images were

loaded into dedicated software (NRecon1.6.3.2, Bruker microCT, Kontich, Belgium) to reconstruct virtual cross-sections of the sample. This resulted in a 3D greyscale datastack, digitized to 880 slices of 2000 by 2000 pixels. The images were smoothed by a Gaussian smoothing kernel, and corrected for rings and beam hardening, which are common artifacts in X-ray CT images. For image analysis a cylindrical volume of interest (diameter 2.5 mm) was cropped centrally in the imaged volume to exclude interference with the excised borders of the sample. The remaining volume for analysis measured 5.4 mm^3. The images were filtered in 3D space using a median filter with filter radius of 2 pixels. Otsu's algorithm (Otsu, 1979) was applied for binarizing the image by separating two peaks in the grey scale frequency distribution: pixels with lower intensities than the Otsu threshold were assigned to the background (air) and pixels with a higher intensity than that threshold were assigned to the apple tissue material. Individual 3D objects smaller than 27 voxels were considered to be noise and were filtered out of the datastack. Morphometric parameters describing the microstructure were calculated on the 3D data using CTAn v.1.12.0.0 (Bruker microCT, Kontich, Belgium). A description of the parameters and the main concept of the calculation can be found in Herremans et al. (2013) and Skyscan (2010).

2.3.2 Optical coherence tomography

All measurements have been performed with a modular spectral domain OCT system (henceforth referred to as "SD-OCT"), which is composed of a light source, a probe head and a spectrometer. The supercontinuum light source (Koheras SuperK Versa, NKT Photonics, Denmark) emits light at a central wavelength of 860 nm. Its spectral bandwidth of 170 nm allows for an axial resolution of 2 µm (in air). In the probe head, the beam is split by a non-polarizing bulk beam splitter (BS) into a reference and a sample arm. In the reference arm light is reflected from a gold coated mirror (M), whereas in the sample arm it is reflected from the different layers within the sample. The light returning from both arms is recombined and sent to the spectrometer, where it is spectrally dispersed by a transmission grating and recorded by a CCD camera. The recorded spectrum is modulated by interference fringes, with the frequency of the modulation depending on the path length differences between reference and sample arm. For recording a cross-section image the beam of light is scanned over the sample surface over a range of 5 mm by means of a

galvanometer mirror (GM). During this process 1000 interferograms are recorded, which are used for reconstructing the images. A schematic diagram of a spectral-domain OCT system is depicted in **Fig. 1**. This particular system was equipped with a multi focal-length probe head. With such a probe head it was possible to switch between different imaging optics, and thus, to change the lateral resolution and depth of focus of the probing beam. Single depth scans were acquired at a rate of 20 kHz.

2.4. Texture and sound emission analysis

A TA-XT plus Texture Analyzer (Stable Micro Systems, Godalming, UK) was used for bending-snapping test fitted with a 50N load cell and equipped with an acoustic emission detector (AED, Stable Microsystems), using the HDP/3PB Three Point Bending Rig. The lower supporting blades were separated by a distance of 45 mm, and the compressing blade was driven down between the two supports at a speed of 0.17 mm/s, bending each apple ring until it snapped. A microphone unit Type 4188-A-021 (Brüel & Kjær) was connected to an AED for sound pressure measurements and was placed at the sample level located 100 mm away from the central axis of the probe. The sound measurement system was calibrated using the Brüel & Kjær Type 4231 sound calibrator at sound pressure levels of 94 and 114 dB at 1000 Hz. The gain of AED was set at 0 dB and the sampling rate was set at 500 Hz for sound and force measurements. Acoustic signals were captured in "RAW" format used in the TA.XT plus Texture Analyzer. Data were than converted to dB. The mechanical and acoustic characteristics were extracted from the data using Texture Exponent 32 software (Stable Microsystems). All tests were performed in a laboratory with no special soundproof facilities at room temperature. Force/displacement and sound/displacement curves were simultaneously plotted. From the force curve the following parameters were extracted: number of peaks, ring hardness corresponding to the maximum force (*hardness*, N), distance at the first major point (*Travel1*, mm), distance at the break (*fracturability*, mm), work required to the first major fracture point (*Area1*, N×mm), work required to snap the ring (*Total area*, N×mm), slope of the first part of the force curve (*slope*, N/mm) and gradient to the maximum force (*gradient_max*, N/mm). From the sound curves the following data were extracted: total number of sound peaks (*N_sounds*), number of sound peaks having SPL higher than 60 dB (*N_sounds>60dB*), average SPL of sound peaks lower than

60 dB ($SPL_{av<60}$), average SPL of sound peaks higher than 60 dB ($SPL_{av>60}$), average SPL of total sound peaks (*avSPL*). The crispness index (E_{mod}, MPa) was calculated from *gradient_max* (E_{mod} max) and *slope* (E_{mod} slope) according to Farris, Gobbi, Torreggiani & Piergiovanni (2008).

2.5. Statistical analysis

Data were submitted to Analysis of Variance and means were compared by Tukey's (mechanical and acoustic parameters) and Duncan's (morphometric parameters) tests at P≤0.05% (Statgraphics v.7, Manugistic Inc., Rockville, MD, USA).

Principal Component analysis (PCA) was carried out in order to study the relationships between X-ray CT morphometric parameters and mechanical and acoustic properties of dried rings considering 10 morphometric parameters, 6 mechanical and 5 acoustic parameters and was performed by The Unscrambler X version 10.0.1 (CAMO, Oslo, Norway) software package using the nonlinear iterative partial least-squares (NIPALS) algorithm. The principal component (PC) scores were then submitted to ANOVA, and means were compared by Duncan's test at P≤0.05%.

3. **Results**

3.1 Absorption coefficient at harvest

The absorption coefficient at 670 nm ranged from 0.35 cm^{-1} for the least mature fruit to 0.092 cm^{-1} for the most mature apple; the optical properties at harvest of LeM and MoM apples selected for this study were (average ± standard error): LeM maturity class: 0.032 ± 0.0083 cm^{-1}; MoM maturity class: 0.11 ± 0.0064 cm^{-1}.

3.2. Microstructure

Fig. 2 (left) presents an X-CT slice of an OSMO2 LeM dried apple ring. The skeleton of dried apple tissue could be accurately detected because of the high contrast with the pore space. So, a threshold was applied to segment skeleton from the pore space resulting in a binary image (**Fig. 2, right**). **Fig. 3** shows representative cross sections of noOSMO and OSMO2 MoM dried apple rings. By comparing the images, it is clear that the microstructure of dried apple ring somewhat changes with the osmodehydration pre-

drying. In fact, in the OSMO2 sample an higher presence of large pores than in the noOSMO ones is evident.

Considering the morphometric parameters computed (**Table 1**), on average (mean±standard error) the osmotic pre-treatment increased porosity (noOSMO, 77.8±1.1 %; OSMO2, 82.0±1.6 %) and tissue specific surface area (noOSMO, 144.82±8.61 mm^{-1}; OSMO2, 159.81±2.79 mm^{-1}) and decreased pore anisotropy (noOSMO, 0.532±0.016; OSMO2, 0.499±0.014), tissue thickness (noOSMO, 0.0233±0.0011 mm; OSMO2, 0.0205±0.00034 mm), tissue anisotropy (noOSMO, 0.564±0.012; OSMO2, 0.501±0.012) and tissue intersection surface (noOSMO, 2.67±0.23 mm^2; OSMO2, 1.73±0.13 mm^2). On the other hand, tissue specific surface area and tissue thickness, along with tissue fractal dimension, depended also by the TRS maturity class: in fact LeM rings on average had higher tissue specific surface area (LeM, 159.92±6.58 mm^{-1}; MoM, 144.71±6.12 mm^{-1}) and lower tissue thickness (LeM, 0.0209±0.00083 mm; MoM, 0.0228±0.00113 mm) and tissue fractal dimension (LeM, 2.490±0.012; MoM, 2.527±0.011). In addition, the comparison of the TRS maturity classes within the same pre-treatment highlighted that in noOSMO samples only porosity was influenced by TRS maturity class, with LeM rings showing higher porosity than MoM rings, while in OSMO2 samples LeM rings were characterized by lower pore fragmentation index and tissue fractal dimension, and higher tissue specific surface area, tissue fragmentation index and tissue structure model index than MoM rings. Furthermore, the osmotic pre-treatment had a diverse impact on morphometric parameters in the two TRS maturity classes. In fact, the osmotic pre-treatment induced in LeM rings a decrease in pore anisotropy, tissue anisotropy and tissue intersection surface, whereas in MoM rings an increase in tissue specific surface area and a decrease in tissue thickness and tissue fractal dimension **(Table 1)**.

A more profound insight in the microstructure is shown by the pore space thickness and tissue structure thickness distributions. These are approximated by a 3D sphere-fitting algorithm on the skeletonized structure, hereby calculating local structure diameters for every position on the skeleton.

The tissue thickness distributions (**Fig. 4**) show that more than 75% of cell spaces in OSMO2 rings were smaller than 25 µm, independently from the TRS maturity class. In contrast, for noOSMO rings only 60.2% (MoM) and 72.8% (LeM) of cell spaces were smaller than 25 µm. As for pore space thickness

distributions (**Fig. 5**), in noOSMO rings, whatever the TRS maturity class, more than 50% of pores had thickness smaller than 0.10 mm, and only about 3% of pores were larger than 0.20 mm, with a maximum value of 0.27 mm. With the osmotic pre-treatment, for both LeM and MoM rings the distribution was shifted towards larger values. In LeM rings 39.6% of pores had thickness lower than 0.10 mm, and 8.7% of pores were larger than 0.20 mm, reaching a maximum value of 0.32 mm, whereas in MoM rings only 37% of pores were smaller than 0.10 mm, and more than 17% of pores were larger than 0.20 mm, with about 5.7% of pore thickness ranging from 0.40 to 0.458 mm.

3.3 Subsurface structure

Fig. 6 shows representative OCT images of the subsurface of the dried rings from the least (R1) and most (R20) mature apple fruit in each batch. The shown images consist of 1000 adjacent depth scans and feature (optical) dimensions of 5 × 0.88 mm^2. OCT clearly distinguished noOSMO and OSMO air-dried rings: noOSMO samples feature a dense structure and thus a limited penetration depth, while the OSMO ones feature a loose surface structure with large inclusions of air. The differences between the noOSMO and OSMO samples seemed to be a surface effect, since they could not be clearly reproduced at freshly prepared sites of fractures. From OCT images it was not possible to deduce the time of the osmodehydration pre-treatment or the effect of the TRS maturities.

3.4 Crispness parameters of air-dried and osmo-air-dried apple rings

If the mechanical and acoustic properties of dried rings from the selected fruit are considered (**Table 2**), no significant influence of TRS maturity at harvest within each pre-treatment was found for the parameters taken into consideration, with a few exceptions concerning the acoustic parameters. In noOSMO treatment LeM rings were characterized by higher value of $SPL_{av<60}$ than MoM ones, whereas in OSMO2 samples, LeM rings showed lower values of $SPL_{av>60}$ and *avSPL* than MoM rings.

In contrast, the osmotic pre-treatment strongly influenced some mechanical properties and almost all the acoustic parameters: in OSMO rings *fracturability*, *Area1* and *Travel1* were lower, and *gradient_max*, *slope*, E_{mod}.max and E_{mod}.slope were higher than in noOSMO rings, being in OSMO rings (mean ± standard

error): *fracturability*, 0.66±0.04 mm; *Area1*, 1.70±0.18 N×mm; *Travel1*, 0.51±0.04 mm; *gradient_max*, 11.92±0.69 N/mm; *slope*, 10.72±0.38 N/mm, E_{mod}.max, 279.1±26.5 MPa; and E_{mod}.slope, 252.6±24.6 MPa. No differences in mechanical properties between the times of osmotic pre-treatment were found.

The *N_sounds* did not differ among the pre-treatments, even if there was a tendency to increase with the osmodehydration time, with OSMO2 rings showing a mean value almost twice the value of noOSMO samples. However, OSMO2 rings were characterized by a significantly higher *N_sounds>60dB* (14.3 ± 3.7), higher $SPL_{av<60}$ (50.37 ± 0.45 dB), higher *avSPL* (57.86 ± 0.74 dB), and lower $SPL_{av>60}$ (71.39 ± 1.17 dB), than noOSMO rings, which showed lower *N_sounds>60dB* (4.5±1.4), corresponding to only about 15% of *N_sounds*, lower *avSPL* (51.07±1.69 dB) and $SPL_{av<60}$ (45.86±0.74 dB), but higher $SPL_{av>60}$ (80.00±1.74 dB). The osmosis time significantly influenced $SPL_{av<60}$ and $SPL_{av>60}$, being the former lower in OSMO1 rings (48.40 ± 0.57 dB), value higher than the noOSMO ones, and the latter higher in OSMO1 rings (77.97± 1.56 dB), value not different from the noOSMO..

3.5 PCA on mechanical and acoustic properties and morphometric parameters

PCA based on X-CT morphometric parameters reported in Table1 and the mechanical and acoustic properties of each ring analysed by X-CT allowed the selction of four principal components (PC), which explained 89.8% of total variation (**Fig.7**). In PC1 (45.18% of total variance) *slope*, *gradient_max* and E_{mod} slope mechanical parameters were positively related to *avSPL*, *N_sounds* and *N_sounds>60dB* acoustic parameters and negatively related to $SPL_{av>60}$ and *Area1* parameters. In addition, PC1 highlighted relationships between some morphometric parameters and acoustic characteristics: total porosity was related to $SPL_{av<60}$, and was opposite to tissue anisotropy and pore anisotropy, which were related to $SPL_{av>60}$, while *Area1* was related to tissue intersection surface. PC1 had positive scores for OSMO2 rings, with LeM OSMO2 ones having the highest value, and negative for noOSMO rings, without any difference between the TRS maturity classes (**Fig.8**). PC2 (26.55% of total variance), instead, underlined positive relationships between morphometric parameters and mechanical characteristics: pore fragmentation index was related to *fracturability* and the work required to snap the ring (*Total area*) to specific surface area. Moreover, PC2 opposed pore fragmentation index, *fracturability*, and tissue fractal dimension to tissue

fragmentation index, tissue structure model index, *Total area* and specific surface area, and distinguished dried apple rings according to the TRS maturity class. In fact, PC2 had negative scores for LeM rings and positive scores for the MoM ones, but this difference was statistically significant only for the OSMO2 rings (**Fig.8**). PC3 (10.67% of total variance) was mainly linked to pore anisotropy, $SPL_{av>60}$ total porosity and tissue anisotropy, which were opposite to tissue structure model index and tissue intersection surface, whereas in PC4 (7.48% of total variance) specific surface area was inversely related to *Nsounds>60dB* and *N_sounds* acoustic parameters. PC3 and PC4 distinguished the TRS maturity classes, but only for the noOSMO rings, which were characterized by positive scores for LeM rings and negative scores for the MoM ones (**Fig.8**).

4. **Discussion**

The usefulness of the osmotic step as a pre-treatment prior to air-drying is related to the physico-chemical modifications occurring in the plant tissue. In fact the simultaneous counter-current mass transfer process, in which water outflows to the surrounding solution and the solute infuses into the product, causes in a short time a fully plasmolysis of the cells on the surface of the material due to osmotic dehydration, with little or no influence on the interior cells, so developing a gradient of turgor pressure, which can deform the structure. Shrinkage and stretching forces are not strong enough to break cell walls or to split middle lamella, but, when the osmotic process lasts at least 3 h, some detachments of cells occur, resulting in the deformation and creation of new and small intercellular spaces (Lewicki & Porzecka-Pawlak, 2005). It was shown that osmosis is a surface process as sugars penetrate to a depth of 2-3 mm, where a decreasing of water binding by the apple can be observed (Salvatori, Andrés, Chiralt & Fito, 1999). During subsequent air drying, sugars added during the osmotic dehydration pre-treatment helped to decrease structural collapse (del Valle, Cuadros & Aguilera, 1998; Lewicki, 1998; Lewicki & Lukaszuk, 2000), which resulted in a more porous structure. The OCT analysis, applied in this work for the first time as an alternative imaging method to study the sub-surface structure of air-dried and osmo-air-dried apple rings, confirmed the fact that the osmosis is a surface process, as the differences found by OCT imaging between noOSMO and OSMO rings could not be clearly reproduced at freshly prepared sites of fractures. The observed

386 difference in the subsurface structure, i.e. a dense structure for noOSMO rings and a loose surface structure
387 with large inclusions of air for the OSMO ones, could be due to the fact that upon immersion in the osmotic
388 medium the first layers of cells die, and resulting in the creation of a volume near the surface (Mavroudis,
389 Dejmek &Sjöholm, 2004).
390 Scanning electron microscopy (SEM) studies carried out by Moreno, Simpson, Estrada, Lorenzen, Moraga
391 & Almonacid (2011) on 'Granny Smith' apples showed the effects of osmodehydration in sucrose solution
392 at microstructural levels. In fresh apples tissues are composed of numerous cells and intercellular spaces,
393 with cells closely bound to each other by middle lamella. In these cells, a large vacuole occupies most of
394 the protoplast, and the plasmalemma and tonoplast are close to the cellular wall. Cellular collapse as well
395 as protoplast contraction and cell wall edge distortion were observed as a consequence of
396 osmodehydration. On the other hand, Witrowa-Rajchert and Rząca (2009) found that air-drying at 70°C
397 caused in apple slices (cv 'Idared') changes in the structure properties of the material, bound to physical
398 alteration, such as shrinkage, increased porosity, decreased ability to imbibe water, and damage to
399 microscopic structure. The same authors reported that in fresh tissue half of the population of the cells has a
400 larger cross-section area than 0.034 mm^2, while most of the dried cells have a cross-section area of 0.0025
401 mm^2 with 50% having cross-section areas up to 0.0020 mm^2. SEM images underlined that in air-dried
402 apple rings the shrinkage stress causes numerous breaks of cell walls, with microstructure being
403 characterized by small cavities and very high density, with larger cells only in the boundary area of the
404 slices, suggesting that shrinkage of air-dried apple rings was anisotropic (Witrowa-Rajchert and Rząca,
405 2009; Bai, Rahman, Perera, Smith & Melton, 2002; Lewicki & Jakubczyk, 2004). In addition, there has
406 been reported a strong negative correlation between porosity, computed from apparent and true density
407 values, and volume shrinkage, ranging the porosity from 69 to 74% with 73-76% volume shrinkage values
408 (Witrowa-Rajchert and Rząca, 2009).
409 Our results showed that the pre-drying osmodehydration treatment caused an increase in the porosity and
410 specific surface area of dried rings, which corresponded to lower volume and area shrinkage (data reported
411 in Rizzolo, Vanoli, Cortellino, Spinelli & Torricelli, 2013), confirming the negative correlation between
412 porosity and shrinkage found by Witrowa-Rajchert and Rząca (2009). The osmotic pre-treatment also

413 affected the degree of pore and tissue anisotropy, which are a measure of preferential alignment of the
414 structure, and they are scaled from 0 for total isotropy to 1 for total anisotropy. Here noOSMO rings
415 showed higher pore and tissue anisotropy values than OSMO2 rings; this difference could be ascribed to
416 how apple rings shrank with air-drying. In fact the light microscopy images of the section of two apple
417 rings air dried at 80°C, one after 90 min of osmosis and the other without the osmotic pre-treatment
418 reported by Gobbi, Farris, Limbo & Torreggiani (2012) showed that an important shrinkage took place
419 along the thickness axis in the not pretreated sample,which was characterized also by far fewer voids, with
420 shape not as around as the pre-treated ring. The positive effect of the osmotic pre-treatment on the dried
421 ring structure was confirmed also by the values of tissue fragmentation index, the tissue thickness
422 distribution and pore space thickness distributions, indicating that in OSMO rings there was a more
423 connected solid structure, with a lower local thickness of the cell spaces and an higher proportion of larger
424 pores than in noOSMO rings. These different morphometric characteristics found for air-dried and osmo-
425 air-dried apple rings greatly influenced the mechanical and acoustic parameters considered as indices of
426 ring crispness. *Hardness*, gradient to the maximum force, E_{mod}, *fracturability*, work required to the first
427 force breakdown and work to snap the ring values indicated that air-dried ring were tough (strong and
428 highly deformable), while the osmo-air-dried one were brittle (hard and weak), as previously found by
429 Farris, Gobbi, Torreggiani & Piergiovanni (2008) and Gobbi, Farris, Limbo & Torreggiani (2012). In
430 addition our results showed that *slope*, *gradient_max* and E_{mod} slope mechanical parameters, which had
431 higher values in OSMO rings, were positively related to *N_sounds*, *N_sounds>60dB* and *avSPL*, all
432 acoustic parameters which have been associated to a high sensory crispness (Salvador, Varela, Sanz &
433 Fiszman, 2009; Saeleaw & Schleining, 2011).
434 Also raw material characteristics (cultivar and ripeness degree) have an influence on apple air-dried ring
435 quality. Konopacka & Plocharski (2001) found that prolonging the storage time of apple fruit (i.e.,
436 increasing ripeness) the derived ring showed incresing density and decreasing thickness retention, and that
437 apple rings produced by fruit after picking (less ripe) and also those produced from soft, overripe fruit after
438 storage were harder than those produced from ripe fruit. Higher ring hardness and crispness index were
439 also found by Rizzolo, Vanoli, Cortellino, Spinelli & Torricelli (2011, 2012) in air-dried apple rings

prepared either from fruit classified at harvest as less mature based on μ_a 670 or from fruit processed at harvest. Our results indicate that using less mature apples based on μ_a 670 measured at harvest by TRS, air-dried ring with higher porosity and higher $SPL_{av<60}$ could be produced, as well as osmo-air-dried ring having a more connected solid structure, with lower tissue and pore degree of anisotropy, and defined less crispy by acoustic parameters (lower $SPL_{av>60}$ and lower *avSPL*) than osmo-air-dried rings produced by more mature fruit.

5. **Conclusion**s

X-ray CT images were used to compute microstructural descriptors, OCT images were used to visualize the subsurface structure, and force and sound pressure level profiles were used to evaluate crispness of air-dried apple rings obtained with or without an osmodehydration pre-treatment. Higher crispness index, higher number of sound events and higher average SPL characterized the OSMO rings. Porosity was related to $SPL_{av<60}$, tissue and pore anisotropy to $SPL_{av>60}$, pore fragmentation index to *fracturability* and specific surface area to the work required to snap the ring. By using principal component analysis a differentiation of the drying treatments, as well as of the products according to the TRS maturity class at harvest were obtained. The differences in mechanical and acoustic characteristics between OSMO and noOSMO rings could be also due to the different subsurface structure as found with OCT analysis.

It can be concluded that there is a clear relation between the maturity at harvest nondestructively assessed on intact fruit by TRS, the processing conditions and the microstructure features determined by X-ray CT and OCT, and texture quality (crispness) of dried apple rings. TRS therefore holds a large promise for application as a straightforward sorting tool for obtaining high quality dried apple rings.

Acknowledgements

This publication has been produced with the financial support of the European Union (project FP7-226783 - InsideFood). The opinions expressed in this document do by no means reflect the official opinion of the European Union or its representatives. Alexandra Nemeth and Michael Leitner furthermore acknowledge support from the European Regional Development Fund (EFRE) in the framework of the EU-program

467 REGIO 13, and the federal state of Upper Austria.

468

469 **References**

470 Acevedo, N.C., Briones, V., Buera, P., & Aguilera, J.M. (2008). Microstructure affects the rate of
471 chemical, physical and color changes during storage of dried apple discs. *Journal of Food Engineering, 85*,
472 222-231.
473 Askari, G.R., Eman-Djomeh, Z., & Mousavi, S.M. (2008). Investigation of the effects of microwave
474 treatment on the optical properties of apple slices during drying. *Drying Technology, 26*, 1362-1368.
475 Bai, Y., Rahaman, M.S., Perera, C.O., Smith, B., & Melton, L.D. (2002). Structural changes in apple rings
476 during convection air-drying with controlled temperature and humidity. *Journal of Agriculture and Food*
477 *Chemistry, 50*, 3179-3185.
478 Contini, D., Martelli, F., & Zaccanti, G. (1997). Photon migration through a turbid slab described by a
479 model based on diffusion approximation. I. Theory. *Applied Optics, 36*, 4587–4599.
480 Cubeddu, R., D'Andrea, C., Pifferi, A., Taroni, P., Torricelli, A., Valentini, G., Ruiz-Altisent, M., Valero, C.,
481 Ortiz, C., Dover, C., & Johnson, D. (2001). Time-resolved reflectance spectroscopy applied to the non-
482 destructive monitoring of the internal optical properties in apples. *Applied Spectroscopy, 55*, 1368-1374.
483 Del Valle, J.M., Cuadros, T.R.M., & Aguilera, J.M. (1998). Glass transition and shrinkage during drying and
484 storage of osmosed apple pieces. *Food Research International, 31*, 191-204.
485 Drexler, W., Morgner, U., Kärtner, F.X., Pitris, C., Boppart, S.A., Li, X.D., Ippen, E.P. & Fujimoto, J.G.
486 (1999). In vivo ultrahigh-resolution optical coherence tomography. *Optics Letters, 24*, 1221-1223.
487 Farris, S., Gobbi, S., Torreggiani, D., & Piergiovanni, L. (2008). Assessment of two different rapid
488 compression tests for the evaluation of texture differences in osmo-air- dried apple rings. *Journal of Food*
489 *Engineering, 88*, 484-491.
490 Gobbi, S., Farris, S., Limbo, S., & Torreggiani, D. (2012). Influence of cultivar and process conditions on
491 crispness of osmo-air-dried apple chips. *Journal of Food Process Engineering, 35*, 810-820.
492 Herremans, E., Verboven, P., Bongaers, E., Estrade, P., Verlinden, B.E., Wevers, M., Hertog, M.L.A.T.M.,
493 & Nicolaï, B.M. (2013). Characterisation of 'Braeburn' browning disorder by means of X-ray micro-CT.

494 *Postharvest Biology and Technology, 75*, 114-124.
495 Huang**,** D., Swanson, E.A., Lin, C.P., Schuman, J.S., Stinson, W.G., Chang, W., Hee, M.R., Flotte, T.,
496 Gregory, K., Puliafito, C.A., & Fujimoto, J. G.(1991). Optical coherence tomography. *Science, 254*, 1178-
497 1181.
498 Huang, L.L., Zhang, M., Wang, L.P., Mujumdar, A.S., & Sun, D.F. (2012). Influence of combination
499 drying methods on composition, texture, aroma and microstructure of apple slices. *LWT-Food Science and*
500 *Technology, 47*, 183-188.
501 Konopacka, D., & Plocharski, W.J. (2001). Effect of raw material storage time on the quality of apple
502 chips. *Drying Technology, 19*, 559-570.
503 Kutis, I.S., Sapozhnikova, V.V., Kuranov, R.V., & Kamenskii, V.A. (2005). Study of the morphological
504 and functional state of higher plant tissues by optical coherence microscopy and optical coherence
505 tomography. *Russian Journal of Plant Physiology, 52*, 59-564.
506 Landahl, S., Terry, L.A., & Ford, H.D. (2012). Investigation of diseased onion bulbs using data processing
507 of optical coherence tomography images. *Acta Horticulturae (ISHS), 969*, 261-270.
508 Lee, C., Lee, S.-Y., Kim, J.-Y., Jung, H.-Y., & Kim, J. (2011). Optical sensing method for screening
509 disease in melon seeds by using optical coherence tomography. *Sensors, 11*, 9467-9477.
510 Léonard, A., Blacher, S., Nimmol, C., & Devahastin, S. (2008). Effect of far-infrared assisted drying on
511 microstructure of banana slices: An illustrative use of X-ray microtomography in microstructural
512 evaluation of a food product. *Journal of Food Engineering, 85*, 154-162.
513 Lewicki, P.P. (1998). Effect of pre-drying treatment, drying and redydration on plant tissue properties: a
514 review. *International Journal of Food Properties, 1* (1), 1-22.
515 Lewicki, P.P., & Jakubczyk, E. (2004). Effect of hot air temperature on mechanical properties of dried
516 apples. *Journal of Food Engineering, 64*, 307−314.
517 Lewicki, P.P., & Lukaszuk, A. (2000). Changes of reological properties of apple tissue undergoing
518 convective drying. *Drying Technology, 18*, 702−722.
519 Lewicki, P.P, & Porzecka-Pawlak, R. (2005). Effect of osmotic dewatering on apple tissue structure.
520 *Journal of Food Engineering, 66*, 43-50.

521 Maltini, E., Torreggiani, D., Venir, E., & Bertolo, G. (2003). Water activity and the preservation of plant
522 foods. *Food Chemistry, 82,* 79-86.
523 Mavroudis, N. E., Dejmek, P., & Sjöholm, I. (2004). Osmotic-treatment-induced cell death and osmotic
524 processing kinetics of apples with characterised raw material properties. *Journal of Food Engineering, 63,*
525 47–56.
526 Mayor, L., Silva, M.A., & Sereno, A.M. (2005). Microstructural changes during drying of apple slices.
527 *Drying Technology, 23,* 2261−2276.
528 Meglinski, I.V., Buranachai, C., & Terry, L.A. (2010). Plant photonics: application of optical coherence
529 tomography to monitor defects and rots in onion. *Laser Physics Letters, 7,* 307-310.
530 Mendoza**,** F., Verboven, P., Mebatsion, H.K., Kerckhofs, G., Wevers, M., & Nicolaï, B. (2007). Three-
531 dimensional pore space quantification of apple tissue using X-ray computed microtomography. *Planta,*
532 *226,* 559-570.
533 Mendoza, F., Verboven, P., Ho, Q.T., Kerckhofs, G., Wevers, M., & Nicolaï, B. (2010). Multifractal
534 properties of pore-size distribution in apple tissue using X-ray imaging. *Journal of Food Engineering, 99,*
535 206-215.
536 Moreno, J., Simpson, R., Estrada, D., Lorenzen, S., Moraga, D., & Almonacid, S. (2011). Effect of pulsed-
537 vacuum and ohmic heating on the osmodehydration kinetics, physical properties and microstructure of
538 apples (cv. Granny Smith). *Innovative Food Science and Emerging Technologies, 12,* 562-568.
539 Otsu, N. (1979). A threshold selection method from gray-level histograms. *IEEE Transactions on systems,*
540 *man, and cybernetics, 9,* 62-66.
541 Rizzolo, A., Vanoli, M., Cortellino, G., Spinelli, L., & Torricelli, A. (2011). Quality characteristics of air-
542 dried apple rings: influence of storage time and fruit maturity measured by time-resolved reflectance
543 spectroscopy. *Procedia Food Science, 1,* 216-223.
544 Rizzolo, A., Vanoli, M., Cortellino, G., Spinelli, L., & Torricelli, A. (2012). Potenzialità della spettroscopia
545 di riflettanza risolta nel tempo per l'ottenimento di rondelle di mele essiccate con elevate caratteristiche
546 organolettiche. In: S. Porretta (Ed.) "Ricerche e innovazioni nell'industria alimentare" vol. X, Chiriotti
547 Editori, Pinerolo, pp. 283-288.

548 Rizzolo, A., Vanoli, M., Cortellino, G., Spinelli, L., & Torricelli, A. (2013). Crispness of air-dried apple
549 rings in relation to osmosis time and fruit maturity measured by time-resolved reflectance spectroscopy.
550 InsideFood Symposium, 9-12 April 2013, Leuven (Belgium).
551 Saeleaw, M., & Schleining, G. (2011). A review: Crispness in dry foods and quality measurements based
552 on acoustic-mechanical destructive techniques. *Journal of Food Engineering, 105*, 387-399.
553 Saeys, W., Velazco-Roa, M.A., Thennadil, S.N., Ramon, H., & Nicolai, B.M. (2008). Optical properties of
554 apple skin and flesh in the wavelength range from 350 to 2200 nm. *Applied Optics, 47*, 908–919.
555 Salvatori, D., Andrés, A., Chiralt, A., & Fito, P. (1999). Osmotic dehydration progression in apple tissue. I:
556 spatial distribution of solutes and moisture content. *Journal of Food Engineering, 42*, 125-132.
557 Salvador, A., Varela, P., Sanz, T., & Fiszman, S.M. (2009). Understanding potato chips crispy texture by
558 simultaneous fracture and acoustic neasurements, and sensory analysis. *LWT – Food Science and*
559 *Technology, 42*, 763-767.
560 Sapozhnikova, V.V., Kamenskii, V.A., & Kuranov, R.V. (2003). Visualization of plant tissues by optical
561 coherence tomography. *Russian Journal of Plant Physiology, 50*, 282-286.
562 Skyscan (2010). Morphometric parameters measured by Skyscan™ software. Available on line at:
563 http://www.skyscan.be/next/CTAn03.pdf.
564 Torreggiani, D., & Bertolo, G. (2004). Present and future in process control and optimization of osmotic
565 dehydration. In: Taylor, S.L. (Ed.), Advances in Food and Nutrition Research, vol. 48: Elsevier, Academic
566 Press, San Diego, pp. 173-238.
567 Torricelli, A., Spinelli, L., Contini, D., Vanoli, M., Rizzolo, A., & Eccher Zerbini, P. (2008). Time-
568 resolved reflectance spectroscopy for nondestructive assessment of food quality. *Sensing and*
569 *Instrumentation for Food Quality and Safety, 2*, 82-89
570 Vanoli, M., Zerbini, P.E., Rizzolo, A., Spinelli, L., & Torricelli, A. (2010). Time-resolved reflectance
571 spectroscopy for the non-destructive detection of inner attributes and defects of fruit. *Acta Horticulturae,*
572 *877*, 1379-1386
573 Verboven, P., Nemeth, A., Abera, M.K., Bongaers, E., Daelemans, D., Estrade. P., Herremans, E., Hertog,
574 M., Saeys, W., Vanstreels, E., Verlinden, B., Leitner, M., & Nicolaï, B. (2013). Optical coherence

575 tomography visualizes microstructure of apple peel. *Postharvest Biology and Technology, 78*, 123-132.
576 Witrowa-Rajchert, D., & Rząca, M. (2009). Effect of drying method on the microstructure and physical
577 properties of dried apples. *Drying Technology, 27*, 903-909.
578 Wolf, W., Behsnilian, D., & Speiss, W.E.L. (2001). Osmotic Dehydration. *Special Issue, Journal of Food*
579 *Engineering, 49*(2-3), 75-270.
580

Table 1. 3-D morphometric parameters (means ± standard error) for noOSMO and OSMO2 dried apple rings in function of TRS maturity class (LeM=less mature; MoM=more mature) (n=2) for tissue structure and pore space.

	Means ±standard error				ANOVA [¥]		
	noOSMO		OSMO2		main effects		Interaction
	LeM	MoM	LeM	MoM	O	M	O×M
Porosity (%)	79.63±0.82	76.04±0.81	81.88±0.76	82.03±3.74	*	ns	ns
Pore anisotropy	0.556±0.013	0.508±0.016	0.470±0.016	0.490±0.028	*	ns	ns
Pore specific surface area (mm^{-1})	42.56 ±1.65	45.15±1.39	39.71±1.85	37.87±9.03	ns	ns	ns
Pore fragmentation index (mm^{-1})	–13.83±17.18	–1.71±9.50	–6.14±1.75	0.17±1.25	ns	ns	ns
Tissue specific surface area (mm^{-1})	155.42±14.80	134.21±0.79	164.42±0.17	155.20±2.03	*	*	ns
Tissue thickness (µm)	21.8±1.6	24.7±0.7	20.0±0.1	21.0±0.5	**	*	ns
Tissue anisotropy	0.582±0.009	0.547±0.016	0.493±0.014	0.509±0.024	**	ns	ns
Tissue Intersection surface (mm^2)	2.36±0.06	2.98±0.34	1.70±0.18	1.76±0.27	**	ns	ns
Tissue fragmentation index (mm^{-1})	–2.58±10.76	–12.10±11.43	–13.36±0.53	–20.24±2.10	ns	ns	ns
Tissue structure model index	0.29±0.38	0.06±0.37	0.012±0.027	–0.227±0.035	ns	ns	ns
Tissue fractal dimension	2.496±0.027	2.545±0.007	2.484±0.001	2.510±0.008	ns	*	ns

[¥] O=osmotic pre-treatment; M=TRS maturity class; significance of P-value: **, P≤0.05%; *, P≤0.1%, ns, not significant

589

590 **Table 2**. Mechanical and acoustic parameters (mean±standard error) of air-dried apple rings prepared from
591 apple fruit selected for X-CT and/or OCT analysis in relation to pre-drying treatment (noOSMO, no pre-
592 treatment; OSMO1; 1h osmodehydration; OSMO2, 3 h osmodehydration). Means in the same row
593 followed by different letters are statistically different (Tukey's test, P≤0.05%) (n=6).

594

	Means ±standard error						ANOVA[¥]		
	noOSMO		OSMO1		OSMO2		main effects		interaction
	LeM	MoM	LeM	MoM	LeM	MoM	O	M	O×M
Mechanical parameters									
number of peaks	2.2±0.6^{a}	3.2±0.84^{a}	4.0±1.1^{a}	5.0±1.1^{a}	3.3±0.7^{a}	3.8±0.5^{a}	ns	ns	ns
hardness (N)	5.98±0.55^{a}	6.83±0.61^{a}	6.65±0.65^{a}	7.13±0.37^{a}	7.41±0.33^{a}	6.82±0.54^{a}	ns	ns	ns
fracturability (mm)	0.95±0.06^{ab}	1.06±0.07^{a}	0.59±0.06^{c}	0.61±0.07^{bc}	0.71±0.11^{bc}	0.73±0.08^{abc}	***	ns	ns
gradient_max (N/mm)	6.98±0.81b^{a}	6.40±0.76^{b}	11.49±1.06^{ab}	12.85±2.08^{a}	12.39±0.89^{a}	10.92±1.41^{ab}	***	ns	ns
Area1 (N×mm)	2.68 ±0.19^{ab}	3.26±0.77^{a}	1.25 ±0.35^{b}	2.08±0.45^{ab}	1.68±0.39^{ab}	1.77±0.24^{ab}	**	ns	ns
Total area (N×mm)	3.39±0.52^{a}	3.86±0.52^{a}	3.72±0.42^{a}	3.29±0.55^{a}	3.61±0.47^{a}	3.70±0.57^{a}	ns	ns	ns
Travel1 (mm)	0.94±0.06^{a}	0.96±0.15^{a}	0.39±0.07^{b}	0.57±0.10^{ab}	0.49±0.08^{b}	0.57±0.05^{ab}	***	ns	ns
slope (N/mm)	5.29±0.63^{b}	6.30±0.38^{b}	11.37±1.34^{a}	11.38±1.77^{a}	10.76±0.58^{a}	9.35±0.65^{ab}	***	ns	ns
E_{mod} max (MPa)	132.3±20.8^{bc}	125.5±12.2^{c}	236.7±35.0^{abc}	343.5±80.1^{a}	313.8±49.1^{ab}	222.6±28.4^{abc}	**	ns	ns
E_{mod} slope (MPa)	101.6±19.7^{b}	124.7±8.5^{ab}	235.9±39.8^{ab}	299.6±65.9^{a}	284.9±59.5^{a}	189.8±11.8^{ab}	**	ns	ns
Acoustic parameters									
N_sounds	23.2±7.6^{a}	25.2±8.7^{a}	33.5±11.4^{a}	30.0±8.6^{a}	48.2±15.0^{a}	40.0±9.7^{a}	ns	ns	ns
N_sounds>60dB	3.5±1.8^{a}	5.5±2.2^{a}	11.5±3.7^{a}	11.7±2.4^{a}	14.5±5.8^{a}	14.2±5.2^{a}	*	ns	ns
$SPL_{av<60}$ (dB)	47.84±0.46^{b}	43.88±0.79^{c}	48.07±0.88^{ab}	48.73±0.78^{ab}	50.92±0.47^{a}	49.81±0.72^{ab}	***	*	**
$SPL_{av>60}$ (dB)	81.82±3.09^{a}	78.19±1.57^{ab}	76.91±2.11^{ab}	79.03±2.41^{a}	69.00±1.51^{b}	73.78±1.20^{ab}	***	ns	ns
avSPL (dB)	52.62±1.85^{bc}	49.51±2.85^{c}	59.35±2.02^{ab}	63.59±3.59^{a}	56.17±0.92^{abc}	59.54±0.68^{ab}	***	ns	ns

595 [¥] O, osmotic pre-treatment, M. TRS maturity class; significance of P-value: *** P≤0.001%; ** P≤0.01%; * P≤0.05%;
596 ns, not significant.

597

598

599 **List of Figures**

621

622 Figure 1

623

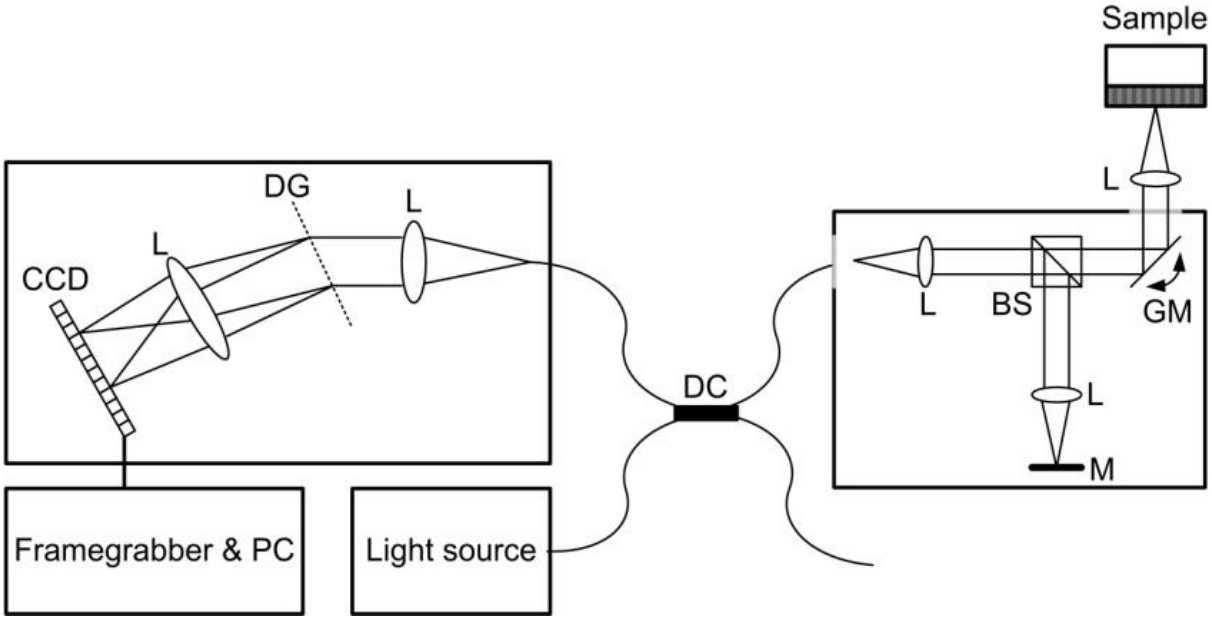

624

625

626

627

628 Figure 2

629

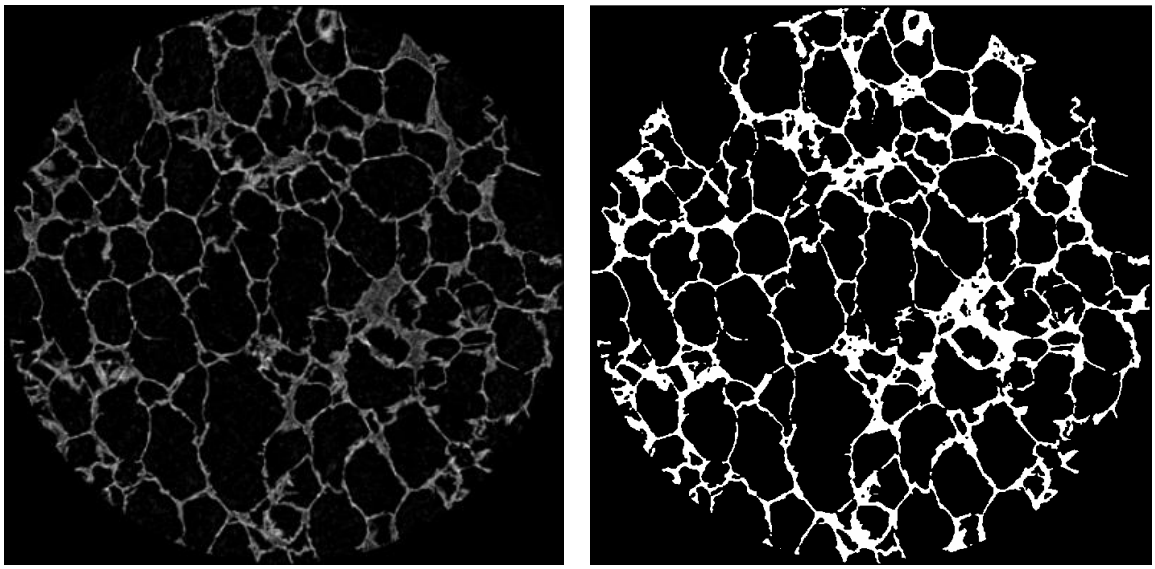

630

631

632

Figure 3.

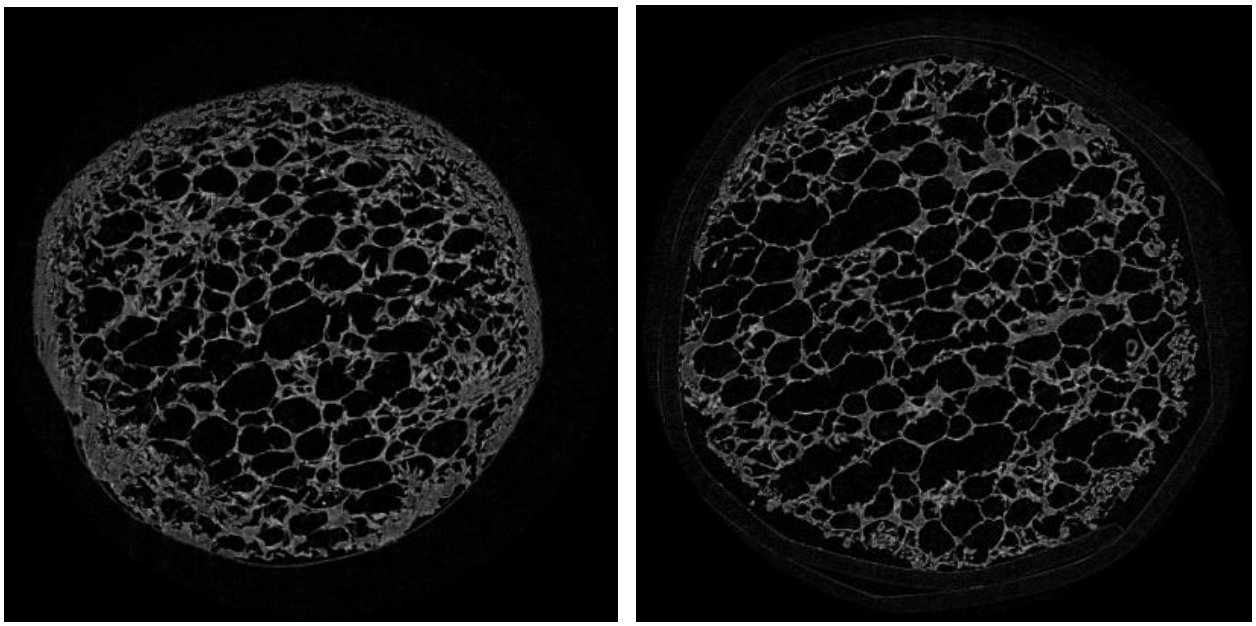

640

641 Figure 4

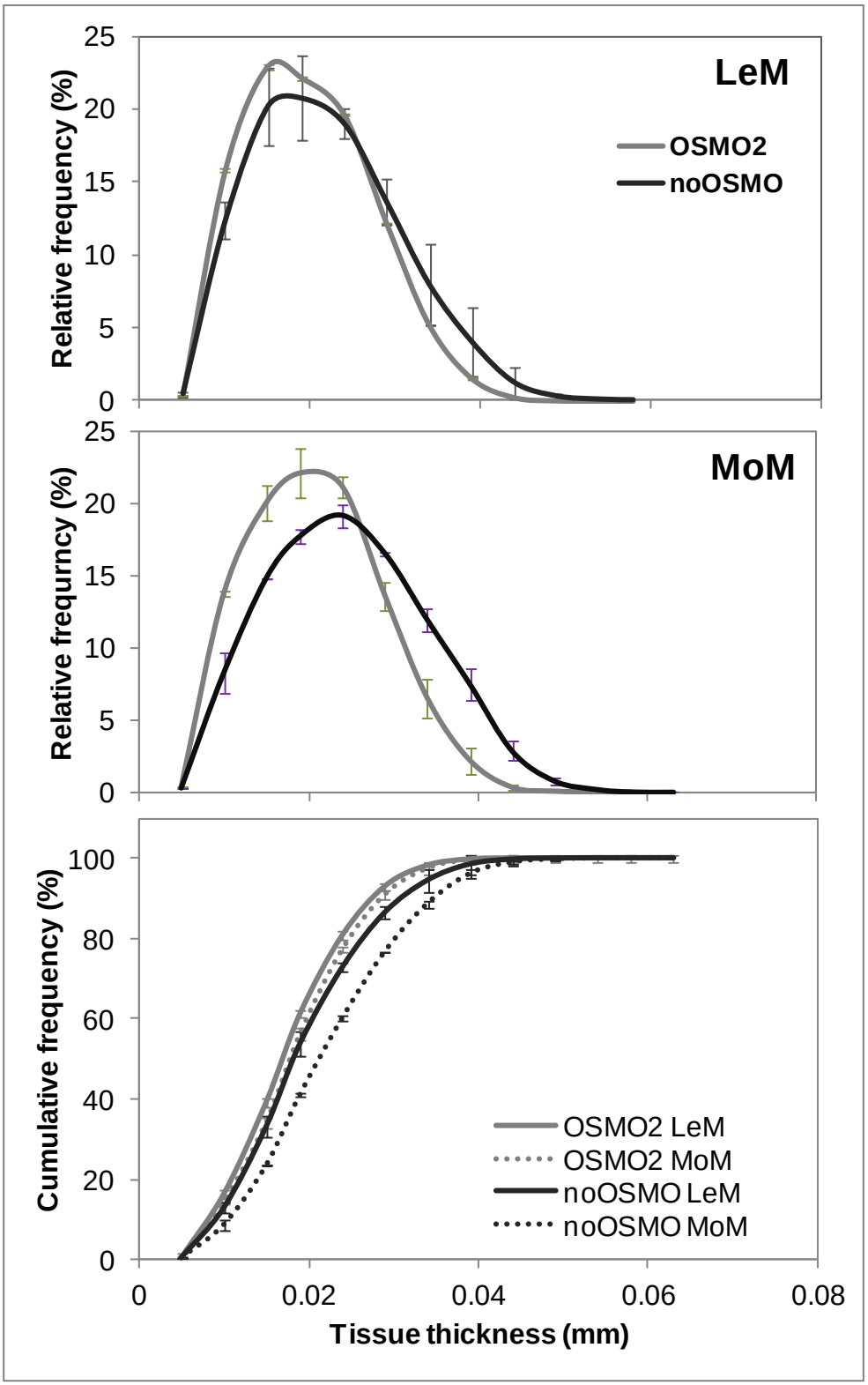

642

643

644

645 Figure 5

646

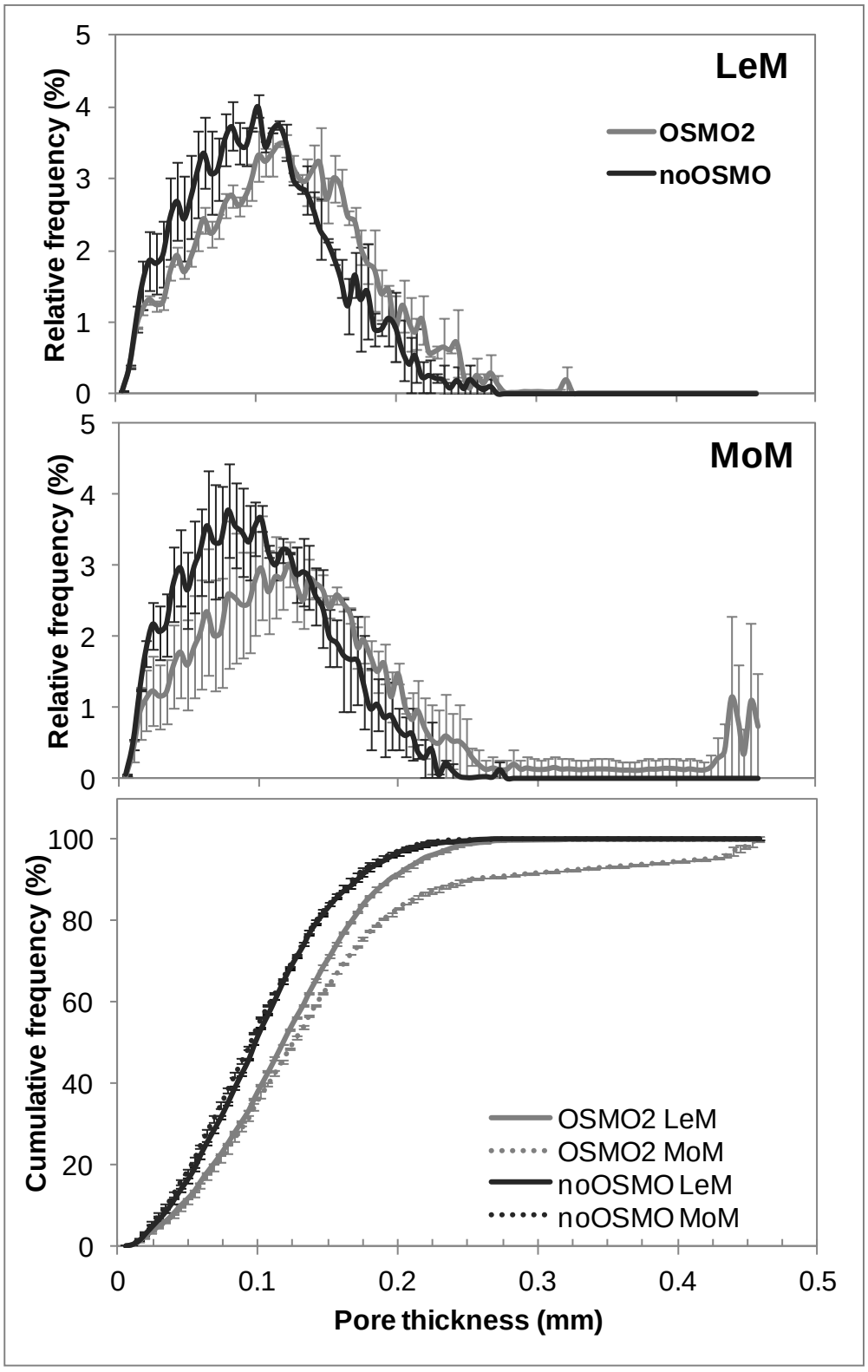

647

648

Figure 6

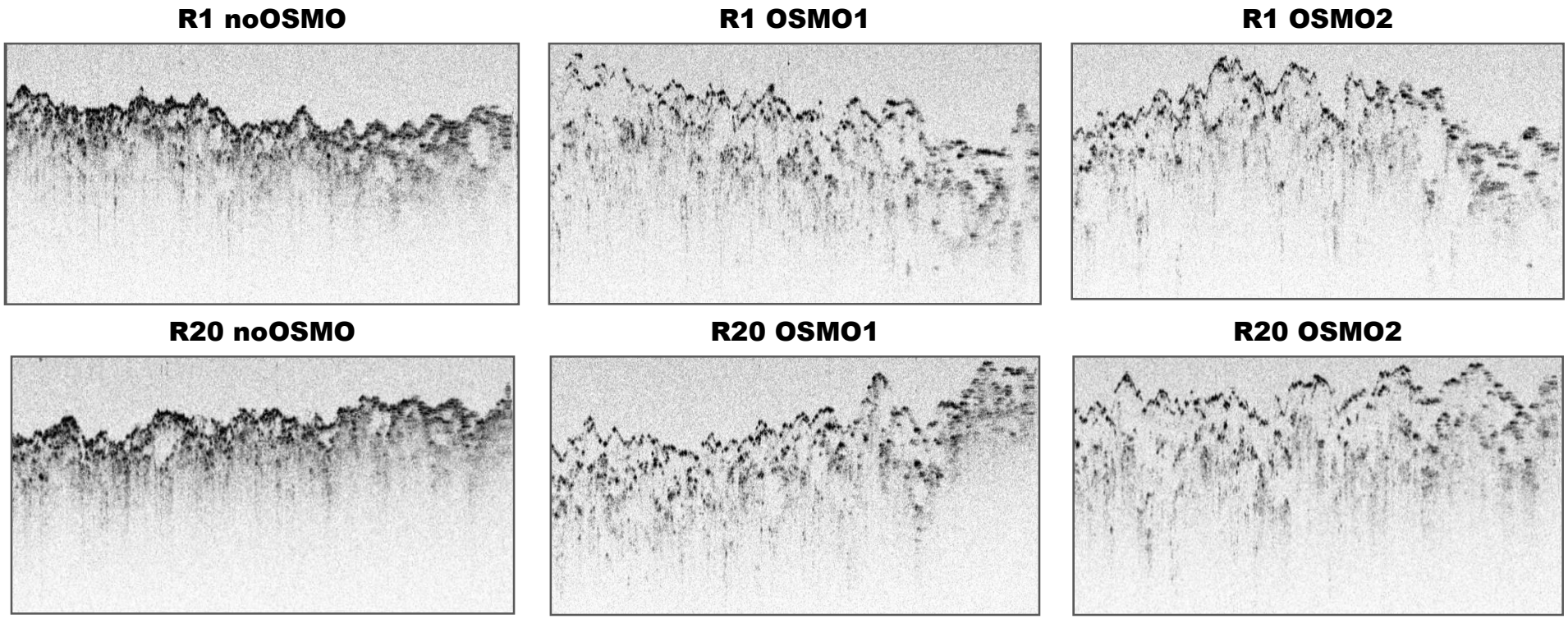

Figure 7

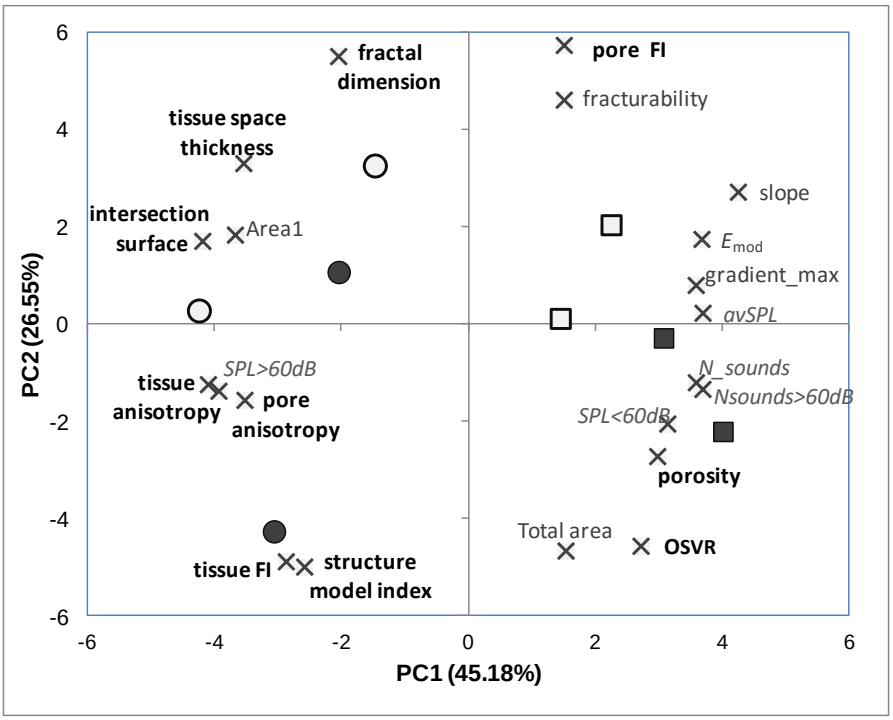
fractal dimension
pore FI
fracturability
tissue space thickness
slope
intersection surface
Area1
E_{mod}
gradient_max
avSPL
SPL>60dB
N_sounds
tissue anisotropy
pore anisotropy
Nsounds>60dB
SPL<60dB
porosity
Total area
OSVR
tissue FI
structure model index
PC2 (26.55%)
PC1 (45.18%)

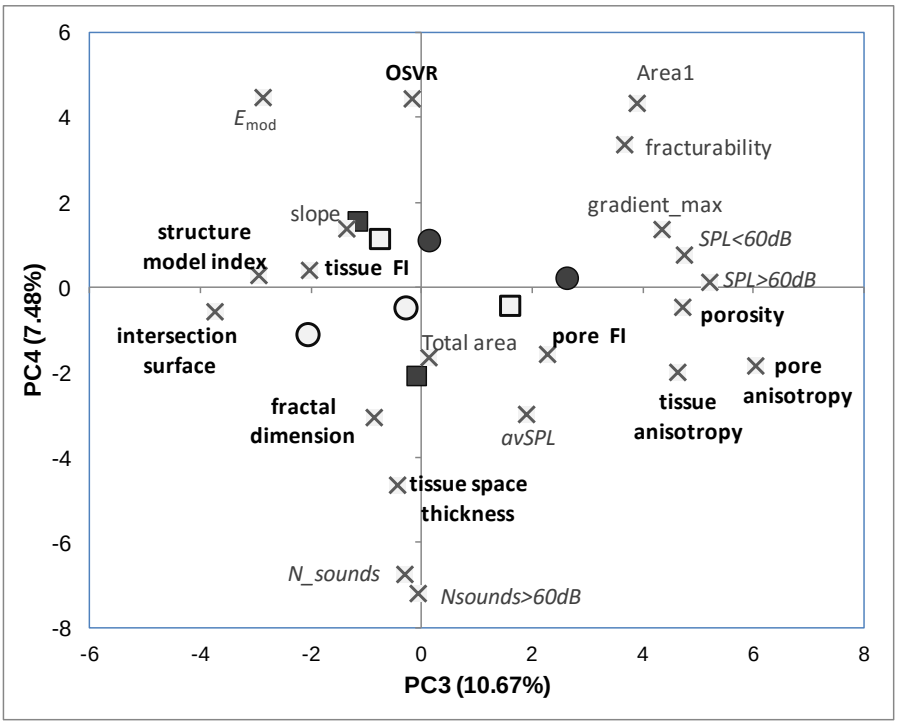
OSVR
Area1
E_{mod}
fracturability
slope
gradient_max
structure model index
tissue FI
SPL<60dB
SPL>60dB
porosity
intersection surface
Total area
pore FI
pore anisotropy
tissue anisotropy
fractal dimension
avSPL
tissue space thickness
N_sounds
Nsounds>60dB
PC4 (7.48%)
PC3 (10.67%)

6 Figure 8

7

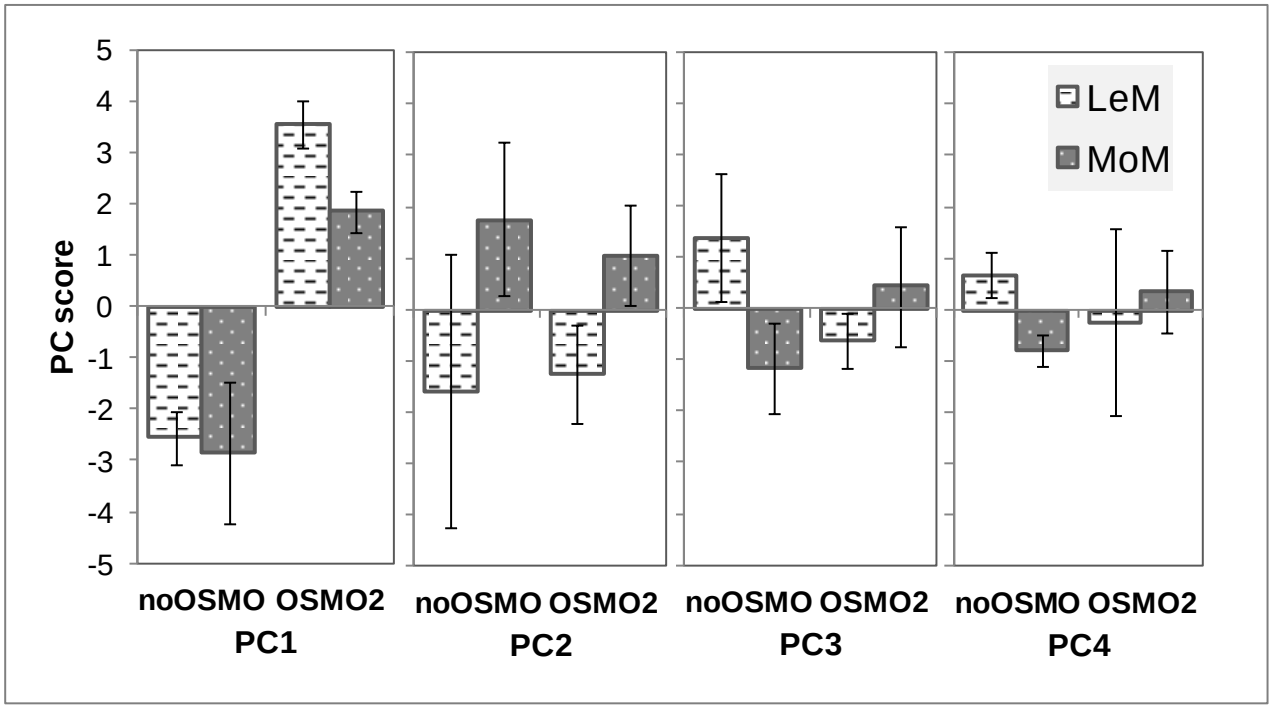
5
4
3
2
1
0
-1
-2
-3
-4
-5
PC score
LeM
MoM
noOSMO OSMO2
PC1
noOSMO OSMO2
PC2
noOSMO OSMO2
PC3
noOSMO OSMO2
PC4

8